CHEMISTRY OF MATERIALS

COMMUNICATION

pubs.acs.org/cm

3-V Full Cell Performance of Anode Framework $TiNb_2O_7$/Spinel $LiNi_{0.5}Mn_{1.5}O_4$

Jian-Tao Han* and John B. Goodenough*

Texas Materials Institute, ETC 9.102, University of Texas at Austin, Austin, Texas 78712, United States

KEYWORDS: lithium-ion battery, $TiNb_2O_7$, $LiNi_{0.5}Mn_{1.5}O_4$

The rechargeable lithium-ion batteries now widely used in cell phones, laptop computers, and digital cameras generally use a graphitic carbon as the anode and lithiated transitional-metal oxide cathodes, for example, $LiCo_{1/3}Ni_{1/3}Mn_{1/3}O_2$, $LiCoO_2$, and $LiFePO_4$,[1−3] because graphite is inexpensive and has better safety characteristics and a longer cycle life compared with a lithium−metal anode. However, like lithium, a charged carbon anode has its electrochemical potential (Fermi energy) poorly matched to the LUMO of the organic liquid-carbonate electrolyte, which is about 1 eV below the Fermi energy of lithium. Therefore, a passivating solid−electrolyte interface (SEI) layer is formed on the carbon to prevent further reduction of the electrolyte. In the case of a carbon anode, a charging voltage V_{ch} electroplates lithium on the SEI layer during a fast charge. On subsequent repeated charges, lithium dendrites extend from the lithium layer; dendrite growth across the electrolyte short-circuits the battery to fire the flammable electrolyte. However, a carbon-buffered alloy having a displacement reaction at a $V \approx 0.8$ V versus Li^+/Li^0 can allow a fast charge.[4] Nevertheless, the formation of a Li^+-permeable passivating SEI layer on the anode increases the impedance of the anode and robs Li from the cathode irreversibly on the initial charge to reduce the limiting capacity of a cell.[5,6] Therefore, there is motivation to identify a large-capacity insertion-compound anode having a voltage range of $1.0 < V \leq 1.5$ V versus Li^+/Li^0.

Among the numerous transition metal oxides that can be used as the anode for lithium batteries, titanium and niobium based oxides continue to be considered promising candidates with beneficial redox potentials Ti^{4+}/Ti^{3+}, Nb^{5+}/Nb^{4+}, and Nb^{4+}/Nb^{3+} ranging from 1.0 to 1.6 V[7−9] that are matched to the LUMO of the organic liquid-carbonate electrolyte. They have considerable safety advantages over the more commonly used metal oxides. On the basis of these considerations, different niobium-based oxides have been explored such as KNb_5O_{13} and $K_6Nb_{10.8}O_{30}$,[9] which exhibit a reversible Li-insertion toward the targeted voltage range of 1.0−1.5 V versus Li^+/Li^0.

More recently, the mixed titanium−niobium oxides such as $Ti_2Nb_2O_9$, $LiTiNbO_5$, and $TiNb_2O_7$[10−13] (TNO) have been investigated as the anode for lithium batteries with some similar electrochemical properties. Importantly, the observed electrochemical performance of carbon-coated $TiNb_2O_7$ (C-TNO) gives a reversible specific capacity of ∼285 (mA h)/g cycled between 1.0 and 2.5 V versus Li^+/Li^0 with over 98% Coulombic efficiency at 0.2 C[13]. Moreover, an SEI layer is formed on discharging to 0.8 V in a half-cell C-TNO/Li, but during subsequent charge/discharge cycles, the C-TNO anode gives a reversible specific capacity of ∼340 (mA h)/g. Here we report tests of a 3-V full cell having C-TNO as the anode and the spinel $LiNi_{0.5}Mn_{1.5}O_4$ (LNMO) as cathode. Single-phase and well-crystallized TNO and LNMO polycrystalline samples were prepared by the same methods reported in previous work.[13−17]

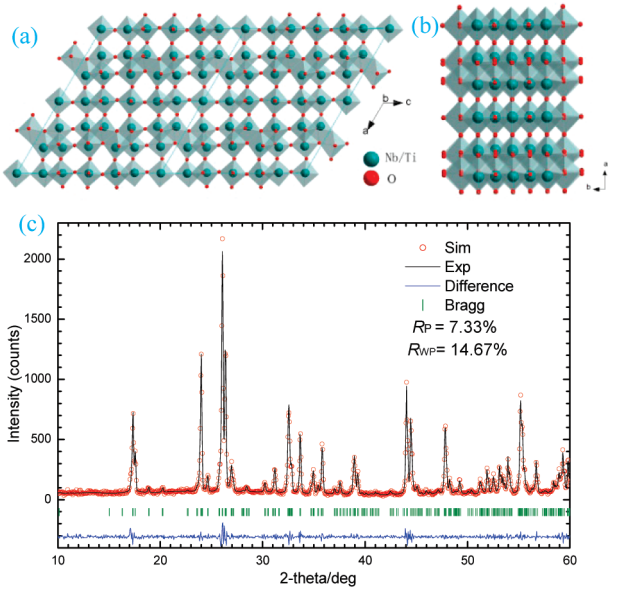

Figure 1. (a) Crystal structure of TNO viewed along the *b* axis and (b) along the *c* axis. (c) Observed (open red circle) and simulated (black solid line) XRD patterns of TNO after Rietveld refinement in the monoclinic space group *C*2/*m* space group, a = 20.3549 (8) Å, b = 3.7992 (2) Å, c = 11.8812 (5) Å, and β = 120.2079 (0)°. The green marks below the pattern give the positions of the Bragg reflections; the difference profile is shown at the bottom.

$TiNb_2O_7$ was first reported by Roth and Coughanour[18] in a paper dealing with phase equilibration in the $TiO_2-Nb_2O_5$ system, which forms a family of block-structure oxides $mMeO_2 \cdot nNb_2O_5$ (Me = Nb^{4+}, Ti^{4+}) known as Wadsley-Roth shear structures; the Ti(IV) and Nb(V) ions are disordered in octahedral sites sharing corners and edges. The limiting composition

Received: May 28, 2011
Revised: June 24, 2011
Published: July 18, 2011

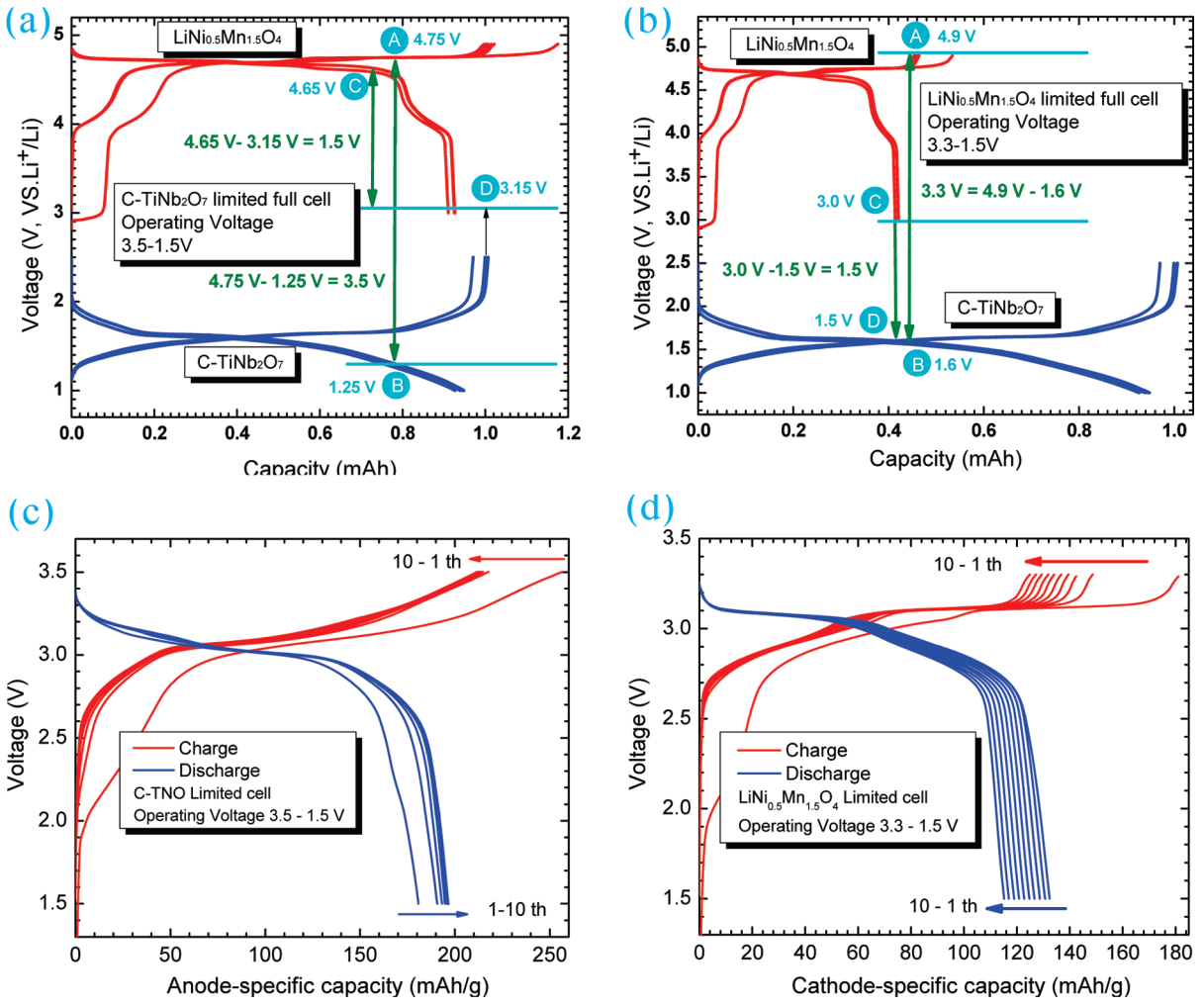

Figure 2. Details of capacity matchup in the C-TNO-limited (a) and LNMO-limited (b) full cell, respectively. The charge and discharge voltage profiles of the C-TNO/Li cells (blue curves) and LNMO/Li (red curves) cells are shown in (a) and (b) with the electrolyte of 1 M $LiPF_6$/EC + DEC (1:1). The cells were operated at the C/10 rate with the cutoff voltages of 1.0−2.5 V for C-TNO/Li cell and 3.0−4.9 V for LNMO/Li cell. (c) Charge/discharge galvanostatic curves for a LNMO/C-NTO cell at C/10 with capacity limited by C-TNO cycled between 1.5 and 3.5 V and (d) for a LNMO/C-NTO full cell at C/10 with capacity limited by the LNMO cathode and cycled between 1.5 and 3.3 V.

Me_3O_7 of the family $mMeO_2{\bullet}nNb_2O_5$, $m = n = 1$, is isostructural with $TiNb_2O_7$; on oxidation, the phase transforms into another structure, the $Me_{12}O_{29}$ block structure, with a lower MeO_2/Nb_2O_5 ratio. The crystal structure of TNO with the highest TiO_2/Nb_2O_5 ratio is illustrated in Figure 1a,b; each metal atom (Ti and Nb) is coordinated to six oxygens forming an octahedral grouping.[19−21] These octahedra are connected through corner and edge sharing to form a crystallographic-shear framework structure. The XRD pattern of the as-obtained TNO sample was refined in the monoclinic space group $C2/m$ ($Z = 6$). The observed, calculated, and difference profiles together with the allowed Bragg reflections are displayed in Figure 1c. The obtained TNO sample is a single phase with lattice parameters $a = 20.3549\ (8)$ Å, $b = 3.7992\ (2)$ Å, $c = 11.8812\ (5)$ Å, and $\beta = 120.2079\ (0)°$, which are in good agreement with those reported in the literature.[19]

Composite electrodes consisting of C-TNO or LNMO (80 wt %), acetylene black (15 wt %) and poly(vinylidene fluoride) (PVDF) (5 wt %) were mixed and rolled into thin sheets and punched into small circular disks with a diameter of ∼7 mm. The electrolyte used for analysis was 1 M LiPF6 in 1:1 = EC/DEC. CR2032 coin cells were assembled in an argon-filled glovebox and then galvanostatically cycled on a multichannel battery cycler (Arbin BTS-2043). The two electrodes were first examined in coin cells with lithium metal as anode (half-cells). The full cells were cycled at a rate corresponding to fully charging the theoretical capacity of the limiting electrode in 10 h (C/10). For all tests of the LNMO/C-TNO full cells, the limiting capacity and the excess capacity of the two electrodes were about 1.0 and 1.2 mA h, respectively.

Figure 2a,b shows, respectively, the details of the capacity matchups of the two electrodes for the C-TNO-limited and LNMO-limited full cells. The red charge/discharge curves for the LNMO electrode show a shoulder near 4.0 V versus Li^+/Li^0 due to the presence of Mn(III) in the as-prepared electrode. The $V =$ 4.75 V on the initial charge corresponds to the formation of a Li^+-permeable SEI layer on the cathode; the HOMO of the electrolyte is about 4.3 eV below the Fermi energy of lithium metal, and an SEI layer is formed on cathodes giving a $V > 4.5$ V. Moreover, overcharging above 4.75 V can lead to an irreversible oxidation of the cathode. The practical specific capacity of the LNMO cathode at C/10 charging rate was ∼120 (mA h)/g, which

dx.doi.org/10.1021/cm201515g |*Chem. Mater.* 2011, 23, 3404–3407

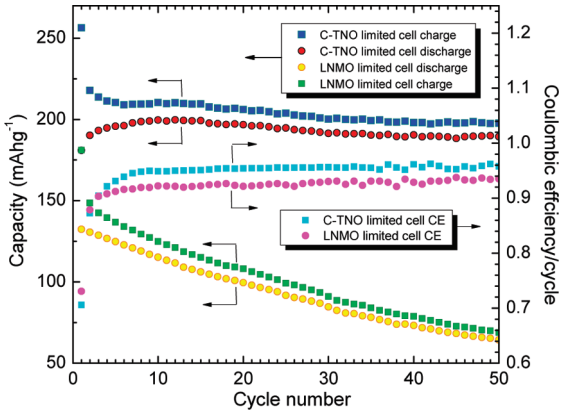

Figure 3. Comparison of the capacity retention of the LNMO/C-TNO cells with capacity limited by the C-TNO anode and LNMO cathode; the Coulombic efficiency/cycle is also shown.

approaches the theoretical 145 (mA h)/g for the extraction of one Li per formula unit. In Figure 2a,b, the capacity is normalized to 1.0 mA h for the anode charge. In the anode-limited cell, the cathode charge is also 1.0 mA h after the initial charge since we discount the excess capacity due to the cathode SEI layer in the initial charge. In the cathode-limited cell, Figure 2b, the capacity of the cathode relative to that of anode is significantly reduced. For the C-TNO-limited cells, the potential of the LNMO cathode remains at 4.75 V versus Li^+/Li^0 at the full-cell cutoff voltage of 3.5 V, point A of Figure 2a, while that of the anode drops to 1.5 V, point B of Figure 2a. However, in the LNMO-limited full cell, the potential of the C-TNO anode is still at 1.6 V at the cell 3.3 V cutoff, but the LNMO cathode potential rises to about 5.0, point A of Figure 2b. Figure 2d shows that at C/10 rate, the LNMO-limited cells are at the end of charge by a cell voltage of 3.2 V; at a 3.3 V cutoff, the cathode is being overcharged.

Figure 2c,d shows, respectively, the voltage profiles and specific capacities, calculated on the mass of the limiting electrode, for the C-TNO-limited full cell over the voltage range $1.5 \leq V \leq 3.5$ V and for the LNMO-limited full cell over $1.5 \leq V \leq 3.3$ V. For the C-TNO-limited cell, there is a charging capacity loss in the initial cycle and then good charging capacity retention on further cycling; conversely, the discharging capacity increases smoothly and then reaches a plateau in the following cycles. However, for the LNMO-limited cell, there is also a charging capacity loss in the initial cycle, and the charging capacity diminishes gradually. Obviously, the cathode is not overcharged in the C-TNO-limited full cell; the capacity is retained on cycling after formation of an SEI layer on the cathode in the initial charge to 3.5 V. In the LNMO-limited full cell, the cathode is overcharged at 3.3 V versus C-TNO to give a capacity fade on repeated cycling.

Figure 3 shows the capacity retention and Coulombic efficiency (CE) of the two kinds of LNMO/LTO cells. The C-TNO-limited cell exhibits a perfect cycling performance in the first 50 cycles with a Coulombic efficiency of more than 95%. However, the LNMO-limited cell gives a poor cycling performance with a capacity loss of 1.5% per cycle and a lower Coulombic efficiency of ~90%. These results show that the C-TNO-limited full cell has a better cycling performance.

As shown in Figure 2a,b, the LNMO/Li cell has a flat operating voltage plateau of ~4.7 V and the C-TNO/Li cell has an operating voltage range of 1.6−1.2 V. The C-TNO anode shows a good stability for almost all of the commercial carbonate-based electrolytes. But most of the electrolytes are apt to be oxidized on the high-voltage LNMO cathode side, especially close to its fully charged state. Thus, for the C-TNO-limited cell at a cutoff voltage range of 1.5−3.5 V, the potential of the LNMO cathode still remains at 4.75 V versus Li^+/Li^0 (point A in Figure 2a), while that of the C-TNO anode drops to 1.5 V (point B in Figure 2a). However, if the cell capacity is limited by the LNMO cathode under the same conditions, the potential of the C-TNO anode is still located at 1.6 V (point B in Figure 2b), but that of the LNMO cathode already rises to about 5.0 V (point A in Figure 2b) where many adverse side reactions occur between the electrolyte and the strongly oxidative cathode. Many studies[22,23] have reported that the full cell of LNMO combined with graphite shows a poor cyclability because the SEI layer of the graphite anode consumes lithium from the LNMO cathode. By substituting graphite with a stable and high capacity C-TNO anode with an operating voltage range of 1.0−1.6 V, we conclude that the C-TNO-limited cell has better overcharge tolerance than the LNMO-limited cell.

In conclusion, we report a framework $TiNb_2O_7$ anode combined with a spinel $LiNi_{0.5}Mn_{1.5}O_4$ cathode to assemble a 3-V LNMO/C-TNO cell system; then two kinds of cell systems whose capacities are limited by the C-TNO anode and the LNMO cathode were investigated. The results indicate that the anode-limited full cell exhibits a better cycling performance than that of the cathode-limited full cells and a longer cycle life than cells with a graphite anode.

AUTHOR INFORMATION

Corresponding Author

*E-mail: jthan0509@gmail.com; jgoodenough@mail.utexas.edu.

ACKNOWLEDGMENT

This work was supported by Office of Vehicle Technologies of the U.S. Department of Energy under Contract No. DE-AC02-05CH11231 and the BATT Program subcontract no. 6805919.

REFERENCES

(1) Yabuuchi, N.; Ohzuku, T. *J. Power Sources* **2003**, *119*, 171–174.
(2) Ceder, G.; Chiang, Y. M.; Sadoway, D. R.; Aydinol, M. K.; Jang, Y. I.; Huang, B. *Nature* **1998**, *392*, 694–696.
(3) Padhi, A. K.; Nanjundaswamy, K. S.; Goodenough, J. B. *J. Eletrochem. Soc.* **1997**, *144*, 1188–1194.
(4) Peled, E.; Tow, D. B.; Merson, A.; Gladkich, A.; Burstein, L.; Golodnitsky, D. *J. Power Sources* **2001**, *97−8*, 52–57.
(5) Hu, J.; Li, H.; Huang, X. *Solid State Ionics* **2007**, *178*, 265–271.
(6) Li, L. F.; Xie, B.; Lee, H. S.; Li, H.; Yang, X. Q.; MeBreen, J.; Huang, X. J. *J. Power Sources* **2009**, *189*, 539–542.
(7) Kang, S. H.; Abraham, D. P.; Yoon, W. S.; Nam, K. W.; Yang, X. Q. *Electrochim. Acta* **2008**, *54*, 684–689.
(8) Anji Reddy, M.; Varadaraju, U. V. *Chem. Mater.* **2008**, *20*, 4557–4559.
(9) Han, J. T.; Liu, D. Q.; Song, S. H.; Kim, Y.; Goodenough, J. B. *Chem. Mater.* **2009**, *21*, 4753–4755.
(10) Colin, J. F.; Pralong, V.; Hervieu, M.; Caignaert, V.; Raveau, B. *Chem. Mater.* **2008**, *20*, 1534–1540.
(11) Colin, J.-F.; Pralong, V.; Caignaert, V.; Hervieu, M.; Raveau, B. *Inorg. Chem.* **2006**, *45*, 7217–7223.
(12) Hervieu, M.; Raveau, B. *J. Solid State Chem.* **1980**, *32*, 161–165.
(13) Han, J. T.; Huang, Y. H.; Goodenough, J. B. *Chem. Mater.* **2011**, *23*, 2027–2029.

(14) Liu, D. Q.; Han, J. T.; Goodenough, J. B. *J. Power Sources* **2010**, *195*, 2918–2923.
(15) Liu, D. Q.; Han, J. T.; Dontigny, M.; Charest, P.; Guerfi, A.; Zaghib, K.; Goodenough, J. B. *J. Electrochem. Soc.* **2010**, *157*, A770–A775.
(16) Liu, J.; Manthiram, A. *J. Electrochem. Soc.* **2009**, *156*, A66–A72.
(17) Liu, J.; Manthiram, A. *Chem. Mater.* **2009**, *21*, 1695–1707.
(18) Roth, R. S.; Coughanour, L. W. *J. Res. Natl. Bur. Stand.* **1955**, *55*, 209–213.
(19) Wadsley, A. D. *Acta Crystallogr.* **1961**, *14*, 660–664.
(20) Gasperin, M. *J. Solid State Chem.* **1984**, *53*, 144–147.
(21) Forghany, S. K. E.; Anderson, J. S. *J. Solid State Chem.* **1981**, *40*, 136–142.
(22) Xiang, H. F.; Zhang, X.; Jin, Q. Y.; Zhang, C. P.; Chen, C. H.; Ge, X. W. *J. Power Sources* **2008**, *183*, 355–360.
(23) Wu, H. M.; Belharouak, I.; Deng, H.; Abouimrane, A.; Sun, Y.-K.; Amine, K. *J. Electrochem. Soc.* **2009**, *156*, A1047–A1050.